INDUCED PROTON PRECIPITATIONS FROM THE INNER RADIATION BELT REGISTERED IN OCEANIA

© 2025 E. A. Ginzburg[a, *], M. D. Zinkina[a, **], and Yu. V. Pisanko[a,b, *]**

[a]*Fedorov Institute of Applied Geophysics, Roshydromet, Moscow, Russia*

[b]*Moscow Institute of Physics and Technology (National Research University), Dolgoprudny (Moscow Region), Russia*

**e-mail: e_ginzburg@mail.ru*

***e-mail: marinaantipina20@mail.ru*

****e-mail: pisanko@ipg.geospace.ru*

Received January 30, 2024

Revised April 10, 2024

Accepted July 25, 2024

Abstract. Detected were induced proton precipitations from the inner radiation belt went with almost a half (11) of 25 anomalous electron events registered onboard "Meteor-M №2" satellite in 2014−2022 in Oceania at low latitudes in the morning hours of local time under quiet geomagnetic conditions. It is surmised that such proton precipitations could be a manifestation of cyclotron resonance between protons and low frequency electromagnetic waves stimulated by a mobile ionospheric heater. Observed effects in anomalous electron events, which could be interpreted in the framework of a mobile ionospheric heater concept, are also discussed.

DOI: 10.31857/S00167940250604e3

1. INTRODUCTION

The inner radiation belt is filled, among others, with energetic protons. It is relatively stable - the average residence time of such protons there is ~ 10 years. Theoretical [Selesnik et al., 2007] and empirical (based on Van-Allen Probes satellite observations) [Selesnik et al., 2018] models of the proton radiation belt have been developed.

Nevertheless, proton outbursts from this belt are occasionally observed. Low-latitude zones of proton bursts at energies of (0.58− 35) MeV have been observed from the OHZORA satellite [Nagata et al., 1988]. Proton bursts with energies up to several MeV from the inner radiation belt were reported [Biryakov et al., 1996] and observed in the orbit of the Mir space station (~ 400 km) near the equator.

The existence near the geomagnetic equator of streams of proton ejections with energies of more than 30 MeV was registered by measurements from the CORONAS-I satellite [Bashkirov et al. [Bashkirov et al., 1999]. The spectra of ejected protons with energies up to 10 MeV near the geomagnetic equator ($L < 1.15$) in low (<1000 km) orbits were measured [Petrov et al., 2008] and modeled [Petrov et al., 2009].

The strong magnetic storm of November 2003 led to an almost complete expulsion of protons with energies of 27− 45 MeV from the inner radiation belt [Selesnik et al., 2013]: the belt was practically emptied. In addition to strong magnetic storms, radiation from ground-based radio transmitters escaping into space was also discussed [Shao et al., 2009] as a possible cause of the observed proton ejections from the inner radiation belt.

According to observations from the Meteor-M No. 2 satellite, 25 anomalous increases of electron fluxes were detected [Ginzburg et al., 2023]. These rare events were registered in 2014− 2022 in Oceania at low latitudes, in the morning hours of local time in calm geomagnetic conditions in energies from ~ 100 keV to several MeV. It is hypothesized that electron ejections from the inner radiation belt were observed: during the bounce oscillations, the electrons fell into cyclotron resonance with radio emission initiated by ground-based and/or ship-based transmitters during the morning local time hours.

The purpose of this report is to search for induced proton ejections (20− 45 MeV) from the inner radiation belt during the above-mentioned 25 electron events and a possible relationship between these proton and electron phenomena.

2. RESULTS OF SATELLITE OBSERVATIONS OF PROTON EJECTIONS

Meteor-M No. 2 meteorological satellite of the Russian Federation was launched on 8.07.2014. The orbit of− is sun-synchronous, altitude at the ascending node $h = 832$ km, inclination $i \sim 98.8°$, orbital period $T = 101.3$ min. The satellite orientation is triaxial, *X-axis* - along the velocity vector, *Z*-axis - from the Earth's center to the satellite, towards the open space.

The satellite instrumentation recording charged particle fluxes included the GALS (developed at IPG) and SCL instruments (developed at the Research Institute of Nuclear Physics of Moscow State University). The GALS instrument had a Cherenkov counter (channel СЧ, registration angle 4π) and two gas-discharge Geiger counters (channels СГ1 and СГ2, registration angles 2π). The SCR instrument had two telescopic DAS1 assemblies. Each assembly consisted of a semiconductor (silicon) detector and a scintillation detector (***CsI***) located behind it on the same longitudinal axis. Table 1 presents the calculated energy characteristics of proton channels D3 and D4, the logic of which was based on simultaneous readings of the semiconductor and scintillation detectors; the separation of proton signals from electron signals in channels D3 and D4 was based on coincidences

and anti coincidences of electric pulses from both detectors with a value proportional to the energy released in them by the passing particle. Angular dimensions of the DAS registration field − 30°.

Table 1.

The assemblies are installed in two mutually perpendicular directions - along the *X-axis* and along the *Z-axis*. In the same Table 1 the energy characteristics of the GALS device channels are also presented. The polling frequency of all channels is 1 s, the accumulation time is 1 s. In order to improve the statistics (especially the statistics of small flows), the readings accumulated for 6 s were used in the future. In the case of small fluxes, they were used directly in the form of the number of particles registered for 6 s. In the case of sufficiently large fluxes, the values expressed in intensity units were used.

In Oceania, the trajectory of the Meteor-M No. 2 satellite runs almost in the direction of the geomagnetic field. Therefore, we chose the DAS1 telescope, mounted along the *X-axis* (along the velocity vector), as the most suitable for studying the induced proton ejections in the observed 25 electron events near the equator. Like any scintillator, ***CsI*** is sensitive not only to protons but also to electrons. The flux of electrons with energies greater than 10 MeV in the inner radiation belt is very small, and with energies greater than 20 MeV− is vanishingly small. Therefore, in channel D4, sensitive to energies of 20 − 45 MeV, only protons are registered. Channel D3 perceives, generally speaking, and electrons with energies greater than 10 MeV.

To study the proton rashes, we used the D4 channel, having collected in one sample the readings of this channel registered in all 25 events under consideration; the total sample volume is 2578 points, each of which corresponds to the number of protons registered in the D4 channel during 6 s. The total volume of the sample is 2578 points.

Fig. 1.

Fig. 1 shows the relative frequency of occurrence plotted against this sample. It can be seen that almost 90% of the time the sensor was "silent"− protons in the channel were not registered, which is related both to the place of observation of the events (on the opposite side of the Earth from the South Atlantic Anomaly, where the magnetic field is elevated) and to the calm geomagnetic conditions when all the events were recorded. The shape of the relative frequency of occurrence suggests an exponential distribution of count rates, and the maximum recorded count rate (2 protons / 6 s) allows us to estimate the exponential distribution parameter λ from the condition that the probability that the count rate does not exceed this maximum is at least 0.99995; this gives $\lambda \approx 5$. In an exponential distribution, the probability of occurrence of the next event neither increases nor decreases with the time counted from the time of registration of the previous event. This justifies the use of such a distribution in describing the random appearance of protons in the orbit of the Meteor-M No. 2

satellite both during the decay of albedo neutrons and as a result of rare proton-Coulomb collisions in the inner radiation belt.

We tested our statistical sample for outliers using the one-way threshold proposed by Dovoedo [2011] for an exponential distribution in the form: $UF=Q_{50}+K(n)(Q_{75}-Q_{50})$, where UF (*upper fence*) is the threshold, $Q_{50} = \ln 2/\lambda$ is the second quantile (median), $Q_{75}=\ln 4/\lambda=2Q_{50}$ is the third quantile, and $K(n)$ is a coefficient depending on the sample size. Following Dovoedo [2011], for our sample we adopted $K(2578) = 13.212$, so that $UF = \ln 2/5 + 13.212\,(2\ln 2/5 - \ln 2/5) = (1+13.212)\ln 2/5 = 14.212 \times 0.13869 = 1.97$, and we considered each exceeding of this threshold in the observational data as an outlier. The values of the coefficients $K(n)$ were tabulated by Dovoedo [2011] by performing numerical experiments with an expression for the probability that one (or more) values from sampling the exponential distribution are incorrectly classified as outliers, given in analytical form (involving, among other things, an incomplete beta function).

Table 2.

Table 2 summarizes 11 of the 25 events considered in [Ginzburg et al., 2023], each of which had at least one emission, i.e., when 2 or more protons were registered in the D4 channel within 6 s.

It turned out that in the 11 events where emissions were observed, protons in the D4 channel were registered much more frequently than in the events where no emissions were observed. Figure 2 shows as examples the D4 channel readings in the 15.08.2016 event− one of the 11 events (left half of Fig. 2) where emissions were observed, and (for comparison) the D4 channel readings in one (22.11.2019) of the other 14 events (right half of Fig. 2) where emissions were not observed. The Cherenkov counter readings are taken as the sign of the events. It can be seen that in the left half of Fig. 2, significantly more pulses were observed in channel D4, including naturally the pulses classified as outliers from the exponential distribution. This may indicate in favor of the fact that in addition to the decay of albedo neutrons and Coulomb collisions of protons in the inner belt, already accounted for within the exponential distribution, something else contributed to the more frequent appearance of protons in the orbit of the Meteor-M No. 2 satellite in the events where the outbursts were observed.

Fig. 2.

3. DISCUSSION

Protons with energies of (20− 45) MeV are nonrelativistic. In Oceania, where the events were recorded, the magnetic field strength in the orbit of the Meteor-M No. 2 satellite varies from 0.25 to 0.29 Gs, which corresponds to a variation of the proton cyclotron frequency from 381.2 to 442.1 Hz.

If we consider the cause of emissions in the D4 channel to be cyclotron resonance of protons residing near the mirror reflection point with electromagnetic waves emitted at frequencies ~ 400 Hz, and take into account that during the local morning hours (~ 8 am), when all 11 events were recorded,

the passage into the inner radiation belt of land-based transmitter signals with frequencies ~ 400 Hz is blocked by the ionosphere [Meredith et al, 2019], then it should be concluded that the only type of ground and/or ship transmitter capable of triggering proton ejections in the local morning− is a heating stand operating at a carrier frequency of 5− 7 MHz (close to the critical frequency of the F2 layer at this time) modulated, in particular, by a frequency of ~ 400 Hz. In this case, the source of radio waves with a frequency of ~ 400 Hz in the internal radiation belt is a diamagnetic current developing in the *F2* layer of the ionosphere along the boundaries of the heating zone, the strength of which oscillates at a modulation frequency of ~ 400 Hz.

With a wide modulation spectrum, the oscillating current arising along the boundaries of the heating zone in the *F2* layer of the ionosphere can generate waves of different frequencies in the inner radiation belt. They are capable, due to cyclotron resonance, to provoke there not only proton precipitations, but also pitch-angle diffusion of electrons into the loss cone at bounce oscillations. The Larmor radius of the belt electrons does not exceed several kilometers, and the length of the trace of the Bouns oscillations of such electrons between the reflection points along the geomagnetic force line is thousands of kilometers, which allows us to geometrically limit ourselves to the approximation of the leading center. The lowest energy of the electrons registered in the events ~ 100 keV suggests a relativistic consideration. Since the wave frequency is less than the electron cyclotron frequency (~ 1 MHz), the belt electrons fall into resonance and approach the ionospheric heating region during the Bauns oscillations. In this case, the cyclotron resonance condition is written in the form:

$$\frac{eB}{m2\pi}(1-\beta^2)^{1/2} = \Omega(1+\beta\cos\alpha)(1-\beta^2)^{-1/2} \quad .(1)$$

Here *e* is the elementary electric charge; *m* is the rest mass of the electron; *B* is the magnitude of the geomagnetic field at the point of interaction between the wave and the electron; α is the angle between the direction of wave propagation and the direction of motion of the leading center of the electron; Ω is the frequency of the wave; $\beta = v/c$, *v* is the velocity of the electron; *c* is the speed of light. In the left part of equation (1) the cyclotron frequency of the electron is written down (taking into account the relativistic increase of its mass), and in the right part− the frequency of the electromagnetic wave shifted according to the relativistic Doppler effect (taking into account that the electron moves towards the wave).

Rewriting (1) in the form:

$$\beta^2 + \frac{2\pi m\Omega}{eB}\beta\cos\alpha - 1 + \frac{2\pi m\Omega}{eB} = 0$$

$$\beta_{1,2} = -\frac{\pi m\Omega}{eB}\cos\alpha \pm \left[\left(\frac{\pi m\Omega}{eB}\cos\alpha\right)^2 + 1 - \frac{2\pi m\Omega}{eB}\right]^{1/2}$$

and considering that $(\frac{2\pi m\Omega}{eB})$ << 1, 0 < β < 1, we obtain:

$$\beta = 1 - \frac{\pi m\Omega}{eB}\cos\alpha$$

$$\Omega = \frac{eB}{\pi m\cos\alpha}(1-\beta).$$

It follows that to get into cyclotron resonance for electrons with energies of 8 MeV and higher (Cherenkov counter CCH) the modulation frequency should be ~ 3 kHz and lower, for electrons with energies of 2.1 MeV and higher (Geiger counter SG2) ~ 30 kHz and lower, and for electrons with energies of 0.8 MeV and higher (Geiger counter SG1) ~ 125 kHz and lower. This means that, in addition to cyclotron resonance of electrons at subharmonics of the carrier frequency (5− 7 MHz) [Ginzburg et al., 2023], assumed in all 25 events, cyclotron resonance is also possible in 11 of the 25 events at waves that are generated at modulation frequencies as well. If in any (of the 11 detected) events the carrier frequency is modulated with kilohertz frequencies in addition to ~ 400 Hz, then a mechanism additional to resonance on subharmonics is involved to stimulate electron precipitations. Consequently, one can expect that the average value of the flux of ejected electrons over these 11 events will be greater than the average value of the flux of such electrons over the remaining 14 events. It should be noted that these 14 events include 3 events during which the D4 proton channel was turned off. These are the events of 25.03. 2019, 31.03. 2019, and 5.04. 2019. We calculated the mean values of the fluxes recorded by the Cherenkov counter (SC) and the two Geiger counters (SG1, SG2) separately for the 11 events in which emissions were observed and for the remaining 11 events (14 − 3) in which no emissions were observed. We also calculated the corresponding standard deviations. The results are summarized in Table 3.

Table 3.

Table 3 shows a tendency in each of the three GALS channels to increase the average flux for the 11 events in which emissions were observed compared to the average flux for the 11 events in which emissions were not observed. This trend may indicate the presence of units and tens of kilohertz among the modulating frequencies, in addition to hundreds of hertz, in one or another of the 11 identified events in which emissions were observed. Table 3 also shows that the standard deviations for two of the three GALS channels (SG2 and MF) were smaller than the average values, and the elucidation of the reason for the large standard deviations for the SG1 channel showed that this is − a consequence of the bell-shaped profile of its readings during the events, in contrast to the almost rectangular profiles of the readings of MF and SG2 (see Fig. 1 [Ginzburg et al., 2023]).

The location of known ground-based heating stands [Streltsov et al., 2018] precludes their use in Oceania, where the Meteor-M No. 2 satellite has recorded 25 anomalous rash events. In the literature [Papadopoulos, 2015; Esser et al., 2017, 2018; Eliasson and Papadopoulos, 2017, 2018], the feasibility of a sea-based mobile heating stand was reported, including for studies in the geomagnetic equator region. Such a bench could heat the *F2* layer of the ionosphere. The diamagnetic current at the boundaries of the heating zone is able (through the magnetic sound generated by this oscillating current) to induce secondary (oscillating at the same frequency) currents in the *E* region [Papadopoulos et al., 2011a, b; Eliasson et al., 2012, 2018; Sharma et al., 2016; Vartanyan et al., 2016; Eliasson and Papadopoulos, 2017]. When operating near the geomagnetic equator, secondary oscillatory currents in the *E*-region are induced directly under the heating zone of the *F2* layer [Papadopoulos et al., 2011a; Eliasson et al., 2012; Wang et al., 2016; Eliasson and Papadopoulos, 2016]. The secondary currents feed the Earth− ionosphere waveguide with electromagnetic waves at the modulation frequency, and generate Alven waves of the same frequency that escape into the inner radiation belt [Shao et al., 2009; Papadopoulos et al., 2011 a, b; Eliasson et al., 2012; Wang et al., 2016; Gekelman et al., 2019]. Cyclotron resonance with Alven waves at frequencies of tens of Hertz, which arises when inner radiation belt protons move along the geomagnetic field toward the heating zone, will lead to their pitch-angle diffusion into the loss cone [Shao et al., 2009]. Perhaps this resonance explains the bell-shaped shape of the reading profile of the SG1 channel, which perceives not only electrons with energies greater than 0.8 MeV, but also protons with energies greater than 15 MeV (Table 1), of which there are about an order of magnitude more in the inner belt than protons with energies greater than 25 MeV registered in the SG2 channel. The precipitation at baunce oscillations of protons can be triggered by a floating heating stand if frequencies of tens of Hertz are also present among the modulating ones.

Engineering studies of mock-ups of the specialized antenna system [Esser et al., 2017, 2018] and the electrical power take-off circuit from the power source to the antenna system [Narayan, 2020] demonstrate that it is feasible to place the mobile heating stand on three steel sea barges of 120 × 32.2 m each. In the extreme case, even two such barges could suffice. In this last variant, the area of the heating stand heating zone in the ionosphere is estimated to be ~ 2500 km^2 [Esser et al., 2018].

The oscillating diamagnetic current flowing along the boundaries of the heating zone in the *F2* layer generates electromagnetic waves at modulation frequencies, and the constant component of this diamagnetic current changes the near-Earth space magnetic field during ionospheric heating. We modeled the main features of such a change by the superposition of the field of the central terrestrial dipole and the field of a solenoid located at the geomagnetic equator at an altitude of 300 km in the *F2* layer and oriented along the dipole force line (the regions where the events were observed appear to be elongated along geomagnetic force lines [Ginzburg et al., 2023]). This ("vacuum") approach

has been used earlier [Shabansky, 1965] (when modeling the magnetic field on the day side of the magnetosphere by superposition of two dipoles) and [Triskova and Veselovsky, 1992] (when modeling the magnetic field of the outer heliosphere by superposition of a dipole and a constant uniform field). In our case, the superposition is justified by the fact that the magnetic field in the inner radiation belt under quiet geomagnetic conditions is practically potential [Tverskaya, 2004]. We calculated the field outside the solenoid following Callaghan and Maslen [1960]. We took the diameter of the solenoid to be ~ 10 km [Streltsov et al., 2018], so that the solenoid length of ~ 250 km was determined based on an estimate of the area of the heating zone in the ionosphere to be ~ 2500 km^2 [Esser et al., 2018]. We estimated the surface diamagnetic current density of the solenoid from the condition of total (thermal plus magnetic) pressure balance at the interface between the heated and unheated (background) ionospheric plasma:

$$n_{i\text{ф}}kT_{i\text{ф}} + n_{e\text{ф}}kT_{e\text{ф}} + \frac{B_{\text{ф}}^2}{8\pi} = n_{i\text{н}}kT_{i\text{н}} + n_{e\text{н}}kT_{e\text{н}} + \frac{B_{\text{н}}^2}{8\pi} \quad . (2)$$

Here k is the Boltzmann constant; ($n_{i\text{f}}$, $n_{e\text{f}}$, $T_{i\text{f}}$, $T_{e\text{f}}$, B_{f}) - ion and electron concentrations, ion and electron temperatures, magnetic field strength at the interface on the background plasma side; ($n_{i\text{н}}$,, $n_{e\text{н}}$,, $T_{i\text{н}}$,, $T_{e\text{н}}$,, $B_{\text{н}}$) − ion and electron concentrations, ion and electron temperatures, magnetic field strength at the interface on the heated plasma side. We consider the ionospheric plasma to be quasi-neutral; for the estimates, we assume that during heating the electron concentration increases by 50% on average, the electron temperature by ~30%, and the ion temperature is practically unchanged [Streltsov et al., 2018].

$$n_{i\text{ф}} = n_{e\text{ф}};\ n_{i\text{н}} = n_{e\text{н}};\ n_{\text{ен}} = n_{e\text{ф}} + \frac{1}{2}n_{e\text{ф}};\ T_{\text{ен}} = T_{e\text{ф}} + \frac{1}{3}T_{e\text{ф}};\ T_{i\text{н}} = T_{i\text{ф}} \quad . \qquad (3)$$

From relations (2) and (3), taking into account $B_{\text{f}} + B_{\text{n}} \approx 2B_{\text{f}}$, we obtain

$$B_{\text{ф}} - B_{\text{н}} = \frac{4\pi}{B_{\text{ф}}}n_{e\text{ф}}k\left(\frac{1}{2}T_{i\text{ф}} + T_{e\text{ф}}\right).$$

Then the surface current density at the interface between the heated and unheated regions (i):

$$i = \frac{c}{4\pi}\left(B_{\text{ф}} - B_{\text{н}}\right) = \frac{c}{B_{\text{ф}}}n_{e\text{ф}}k\left(\frac{1}{2}T_{i\text{ф}} + T_{e\text{ф}}\right) . (4)$$

The critical frequency of the *F2* layer (5− 7) MHz in Oceania in the morning hours of local time (~8 am) corresponds to $n_{e\text{f}} = 4.5\cdot10^5$ cm^{-3} at foF2 = 6 MHz. Taking $T_{e\text{f}} = 2500$ K, $T_{i\text{f}} = 1000$ K, $B_{\text{f}} = 0.25$ Gs, from (4) we find $i \approx 0.075$ A/m^2. Then the total current per unit length of the solenoid of 1 meter is 2 π 750 A/m. Fig. 3 shows the results of calculation of the dependence of magnetic field on magnetic latitude for the superposition of dipole and solenoid (solid line) and dipole (dashed line) for L = 1.1. It can be seen that the presence of solenoid (modeling the magnetic effect from the floating heating bench) changes the magnetic field at small L. The field increases within ~ 3°magnetic latitude from the equator– of the stand dislocation site (in the considered model case the stand was placed on the magnetic equator), and further it turns out to be less dipole-like up to latitude ~ 10°.

Fig. 3.

When registering events, we are talking about the appearance of electrons at a point of the force line distant from the apex of this line. In the absence of an electromagnetic wave, particles with conventionally small bounce amplitudes are grouped near the top of the force line. Exposure of the wave to these particles initially distant from the Meteor-M No. 2 satellite leads to isotropization of their pitch-angle distribution, or, what is the same, to an increase of the bouns-amplitude, including such an increase that the particles can descend to the height of the Meteor-M No. 2 satellite orbit and below. Some of them are capable of reaching the atmosphere - these are precipitating particles. Those that do not get into the loss cone and do not become expelled, will be quasi-captured, registered at a height of ~ 800 km in the zone of the transmitter operation. That is, the GALS sensors register and, generally speaking, do not distinguish between two populations of electrons. First, these are quasi-captured electrons (with such pitch angles that their mirror points are located below the orbit of the Meteor-M No. 2 satellite), which after reflection return back to the radiation belt. Secondly, these are expelled electrons with pitch angles in the loss cone that allow them to be expelled from the radiation belt into the atmosphere. The oscillating diamagnetic current flowing along the boundaries of the heating zone in the *F2* layer causes relativistic electrons to be ejected due to cyclotron resonance at modulation frequencies. This works to increase the number of recorded spitting electrons in addition to those spitting at cyclotron resonance at subharmonics of the carrier frequency (5− 7 MHz). On the other hand, the constant component of the ionospheric diamagnetic current changes the magnetic field at small *L* in the vicinity of the stand dislocation. The changes of the magnetic field raise or lower the height of the mirror points with respect to the orbit of the Meteor-M No. 2 satellite. Changes in the height of the mirror points decrease or increase the number of quasi-captured electrons registered by the GALS sensors. The effect of the magnetic field change on the readings of the GALS sensors is illustrated by the event of 9.07.2017 (Fig. 4).

Fig. 4.

It can be seen that immediately after a typical sharp (lasting several tens of seconds) burst of readings of all GALS sensors at the beginning of the event, associated with an increase in the number of registered trapped electrons, a dip is observed followed by a gradual increase in the count rate of the sensors. The dip can be interpreted as a deficit in the number of registered quasi-captured electrons associated with a local increase (compared to the dipole) of the magnetic field in the vicinity of the stand location due to the contribution of a constant component of the oscillating diamagnetic current flowing along the boundaries of the heating zone. A further increase in the count rate of all sensors, in turn, may indicate a decrease in the total magnetic field with distance from the bench (see Fig. 3) and, accordingly, an increase in the number of registered quasi-captured electrons. All this occurs against the background of an increased number of expelled electrons in the event.

4. CONCLUSION

Approximately half (11) of 25 anomalous electron ejections registered from the Meteor-M No. 2 satellite in 2014− 2022 in Oceania at low latitudes in the morning hours of local time in quiet geomagnetic conditions in energies from ~ 100 keV to several MeV were accompanied by induced proton ejections with energies of 20− 45 MeV. If the cause of the phenomenon is resonance at the proton cyclotron frequency (~ 400 Hz), then (since in the morning hours of local time the passage to space of ground-based signals with frequencies ~ 400 Hz is blocked by the ionosphere) the only type of ground and/or ship transmitter capable of providing the presence of low-frequency electromagnetic radiation in the inner radiation belt in the local morning− is a heating stand. The source of ~ 400 Hz radio waves in the inner radiation belt is a diamagnetic current developing in the *F2* layer of the ionosphere along the boundaries of the heating zone, the strength of which oscillates at a modulation frequency of ~ 400 Hz. Relativistic electrons of the inner radiation belt can also fall into the cyclotron resonance with stimulated low-frequency radiation at a wide range of modulation frequencies. In particular, to get into the cyclotron resonance of electrons with energies of 8 MeV and higher (Cherenkov counter СЧ) the modulation frequency should be ~ 3 kHz and lower, for electrons with energies of 2.1 MeV and higher (Geiger counter СГ2) ~ 30 kHz and lower, and for electrons with energies of 0.8 MeV and higher (Geiger counter СГ1) ~ 125 kHz and lower. The constant component of the oscillating diamagnetic current flowing along the boundaries of the heating zone in the *F2* layer can change the magnetic field at small L during ionospheric heating, which is confirmed by model calculations; this, in turn, will be reflected in the time profiles of the GALS instrument readings.

In the literature [Papadopoulos, 2015; Eliasson and Papadopoulos, 2016], the feasibility of creating a sea-based mobile heating stand has been reported, including for conducting research in the geomagnetic equator region. Engineering studies of mock-ups of the specialized antenna system [Esser et al., 2017, 2018] and the electrical power extraction circuit from the power source to the antenna system [Narayan, 2020] demonstrate that it is feasible to place the mobile heating bench on three steel sea barges of 120 × 32.2 m each.

Therefore, the anomalous electron and proton spikes from the inner radiation belt, registered from the Meteor-M No. 2 satellite in 2014− 2022 in Oceania at low latitudes in the morning hours of local time under calm geomagnetic conditions, allow the interpretation that they are side effects of ionospheric experiments with the use of a floating heating stand.

ACKNOWLEDGEMENTS

We are grateful to three anonymous reviewers for comments and suggestions.

REFERENCES

1. *Ginzburg E.A., Zinkina M.D., Pisanko Yu.V.* Induced electron precipitation from the inner radiation belt recorded in Oceania // Geomagnetism and Aeronomy. V. 63. No. 6. P. 751−763. 2023.
2. *Tverskoy B.A.* Fundamentals of theoretical cosmophysics // Selected works. Moscow: URSS. P. 376. 2004. ISBN 5-354-00647-3.
3. *Bashkirov V.F., Denisov Yu.I., Gotselyuk Yu.V., Kuznetsov S.N., Myagkova I.N., Sinyakov A.V.* Trapped and quasi-trapped radiation observed by CORONAS-I satellite // Radiation Measurements. V. 30. P. 537−546. 1999.
4. *Biryakov A.S., Grigoryan O.R., Kuznetsov S.N., Ryaboshapka A.V., Ryabukha S.B.* Low-energy charged particles at near equatorial latitudes according to MIR orbital station data // Adv. Space Res. V.10. P.10189. 1996.
5. *Callaghan E.E., Maslen S.H.* The magnetic field of a finite solenoid // NASA Technical Note D-465, Lewis Research Center, Cleveland, Ohio, National Aeronautics and Space Administration, Washington, October 1960.
6. *Dovoedo Y.H.* Contributions to outlet detection methods: some theory and applications // A dissertation submitted in partial fulfillment of the requirements for the degree of Doctor of Philosophy in the Department of Information Systems, Statistics, and Management Science in the Graduate School of the University of Alabama, Tuscaloosa, Alabama. P.180. 2011. https://ir-api.ua.edu/api/core/bitstreams/48a91f94-9ee7-4918-8c3c-d1757737ea85/content
7. *Eliasson B., Chang C.-L., Papadopoulos K.* Generation of ELF and ULF electromagnetic waves by modulated heating of the ionospheric F2 region // J. Geophys.-Res. V.117. P.10320. 2012. https://doi.org/10.1029/2012JA017935.
8. *Eliasson B., Papadopoulos K.* HF wave propagation and induced ionospheric turbulence in the magnetic equatorial region // J. Geophys. Res.− Space. V.121. P. 2727−2742. 2016. https://doi.org/10.1002/2015JA022323.
9. *Eliasson B., Papadopoulos K.* Pitch angle scattering of relativistic electrons near electromagnetic ion cyclotron resonances in diverging magnetic fields // Plasma Phys. Control. Fusion. V.59. P.104003. 2017. https://doi.org/10.1088/1361-6587/aa8100.
10. *Eliasson B., Milikh G.M., Liu T.C., Shao X., Papadopoulos K.* Simulations of the generation of energetic electrons and the formation of descending artificial plasma layers during HF heating at Arecibo // J. Geophys. Res.− Space. V.123. P. 10301−10309. 2018. https://doi.org/10.1029/2018JA026073.

11. *Esser B., Beeson S.R., Dickens J.C., Mankowski J.J., Antonsen T.M., Neuber A.A.* The path to a transportable ionospheric heater – tuning methods // IEEE Trans Plasma Sci. V. 45. P. 1051−1057. 2017. https://doi.org/10.1109/TPS.2017.2699925
12. *Esser B., Mauch D., Dickens J., Mankowski J., Neuber A.* Tunable, electrically small, inductively coupled antenna for transportable ionospheric heating // Radio Sci. V. 53. P. 496−508. 2018. https://doi.org/10.1002/2017RS006484
13. *Gekelman W., Pribyl P., Vincena S., Tang S.W., Papadopoulos K.* Ferrite based antennae for launching Alfven waves // Rev. Sci. Instrum. V.90. P. 083505. 2019. https://doi.org/10.1063/1.5103171
14. *Meredith N.P., Horne R.B., Clilverd M.A., Ross J.P.* An investigation of VLF transmitter wave power in the inner radiation belt and slot region // J. Geophys. Res.− Space. V.124. P. 5246−5259. 2019. https://doi.org/10.1029/2019JA026715.
15. *Nagata K., Kohno T., Hasere N., Kikuchi J., Doke T.* Electron (0.19-3.2 MeV) and proton (0.58-35 MeV) precipitations observed by OHZORA satellite at low latitude zones L=1.6-1.8 // Planet. Space Sci. V. 36. P. 591. 1988.
16. *Narayan A.H.* A highly efficient, megawatt class, constant impedance tunable power extraction circuit for mobile ionospheric heaters // Dissertation submitted to the Faculty (Electrical Engineering Department) of the Graduate School of the University of Maryland, College Park in partial fulfillment of the requirements for the degree of Doctor of Philosophy. P. 81. 2020. https://doi.org/10.13016/vhln-r6io
17. *Papadopoulos K., Chang C.-L., Labenski J., Wallace T.* First demonstration of HF-driven ionospheric currents // Geophys. Res. Lett. V. 38. P. 20107. 2011. https://doi.org/10.1029/2011GL049263.
18. *Papadopoulos K., Gumenov N.A., Shao X., Doxas I., Chang C.L.* HF-driven currents in the polar ionosphere // Geophys. Res. Lett. V. 38. P.12103. 2011. https://doi.org/10.1029/2011GL047368.
19. *Papadopoulos K.* Ionospheric modifications using mobile, high power HF transmitters based on TPM technology // Paper presented at 2015 IEEE International Conference on Plasma Science (ICOPS), 24-28 May, Antalya, Turkey. 2015. https://doi.org/10.1109/PLASMA.2015.7179496
20. *Petrov A.N., Grigoryan O.R., Panasyuk M.I.* Energy spectrum of proton flux near geomagnetic equator at low altitudes // Adv. Space Res. V. 41. P. 1269−1273. 2008.
21. *Petrov A.N., Grigoryan O.R., Kuznetsov N.V.* Creation of model of quasi-trapped proton fluxes below Earth's radiation belt // Adv. Space Res. V. 43. P. 654−658. 2009.
22. *Selesnick R.S., Looper M.D., Mewaldt R.A.* A theoretical model of the inner proton radiation belt // Space Weather. V. 5. S04003. 2007. https://doi.org/10.1029/2006SW000275.

23. *Selesnick R.S., Hudson M.K., Kress B.T.* Direct observation of the CRAND proton radiation belt source // J. Geophys. Res.− Space. V. 118. P. 7532−7537. 2013. https://doi.org/10.1002/2013JA019338.
24. *Selesnick R.S., Baker D.N., Kanekal S.G., Hoxle V.C., Li X.* Modeling the proton radiation belt with Van Allen probes relativistic electron-proton telescope data // J. Geophys. Res.− Space. V. 123. P. 685−697. 2018. https://doi.org/10.1002/2017JA024661
25. *Shabansky V.P.* On the first phase of a magnetic storm // Space Res. V.5. P.125−147. 1965.
26. *Shao X., Papadopoulos K., Sharma A.S.* Control of the energetic proton flux in the inner radiation belt by artificial means // J. Geophys. Res. V.114. A07214. 2009. https://doi.org/10.1029/2009JA014066.
27. *Sharma A.S., Eliasson B., Shao X., Papadopoulos K.* Generation of ELF waves during HF heating of the ionosphere at midlatitudes // Radio Sci. 51. P. 962−971. 2016. https://doi.org/10.1002/2016RS005953.
28. *Streltsov A.V., Berthelier J.-J., Chernyshov A.A., Frolov V.L., Honary F., Kosch M.J., McCoy R.P., Mishin E.V., Rietveld M.T.* Past, present and future of active radio frequency experiments in space // Space Sci. Rev. 214:118. 2018. https://doi.org/10.1007/s11214-018-0549-7
29. *Triskova L., Veselovsky I.S.* On the large-scale magnetic field structure in the outer heliosphere / Solar Wind Seven. Ed. E. Marsh, R. Schwenn. New York, London, Seoul, Tokio: Pergamon Press. P. 297−300. 1992.
30. *Vartanyan A., Milikh G.M., Eliasson B., Najmi A.C., Parrot M., Papadopoulos K.* Generation of whistler waves by continuous HF heating of the upper ionosphere // Radio Sci. V. 51. P.1188−1198. 2016. https://doi.org/10.1002/2015RS005892.
31. *Wang Y., Gekelman W., Pribyl P., Van Compernolle B., Papadopoulos K.* Generation of shear Alfven waves by repetitive electron heating // J. Geophys. Res.− Space. V.121. P. 567−577. 2016. https://doi.org/10.1002/2015JA022078.

Table 1. Channel energy intervals of the GALS and SCL instruments

Instrument	Channel	Energy range, MeV	
GALS		protons	electrons
	NF	>600	>8
	SG1	>15	>0.8
	SG2	>25	>2.1
SCR, DAS1		protons	
	Д3	10− 160	
	Д4	20− 45	

Table 2. Events in each of which at least one outlier was observed in the D4 channel readings

Date of event	Number of emissions	L_{start}	L_{end}
13.08.2015	1	1.14	1.14
11.06.2016	1	1.15	1.98
15.08.2016	2	1.42	1.1
30.09.2016	1	1.19	2.02
07.09.2017	2	1.83	1.18
27.12.2019	2	2.94	1.27
11.02.2020	1	1.09	1.25
02.03.2020	1	1.14	1.1
18.01.2021	1	1.22	1.09
24.05.2021	1	1.08	1.22
18.06.2021	2	1.14	1.17

Table 3. Flows in GALS device channels

Channel	11-event average flux (1/cm^{2}with ster) (emissions observed)	11-event average flux (1/cm^{2}with erase) (no emissions observed)
SG1	53.58±99.24	14.20±33.25
SG2	2.77±1.78	2.06±0.82
CH	0.26±0.086	0.23±0.07

Figure captions

Fig. 1. Relative frequency of occurrence of protons in the D4 channel recorded in 25 anomalous events.

Fig. 2. Examples of events when proton emissions were observed in the D4 channel readings (15.08.2016, 20:59:27− 21:07:27 UT) (plots (*a*) and (*c)*), and when no emissions were observed (22.11.2019, 20:59:45− 21:07:03 UT) (plots (*b*) and (*d*)). The value of the McIlwain parameter (*L*) along the trajectory of the Meteor-M No. 2 satellite is plotted along the abscissa axis in all the graphs; the ordinate axes in the upper graphs show the flux intensities, while the lower ones show the number of protons registered in the D4 channel for 6 s. Graphs (*a*) and (*b*) are the Cherenkov counter readings taken as a sign of the event.

Fig. 3. Results of the model calculation of the magnetic field dependence on magnetic latitude for the superposition of a dipole and solenoid (solid line) and a dipole (dashed line). In the considered model case the stand was placed on the magnetic equator.

Fig. 4. GALS sensor readings for the event of 9.07.2017. On the abscissa axis - geographic latitude in degrees, on the ordinate axis - intensities. The magnetic equator for the considered event is located at ~ 6^{o} N.

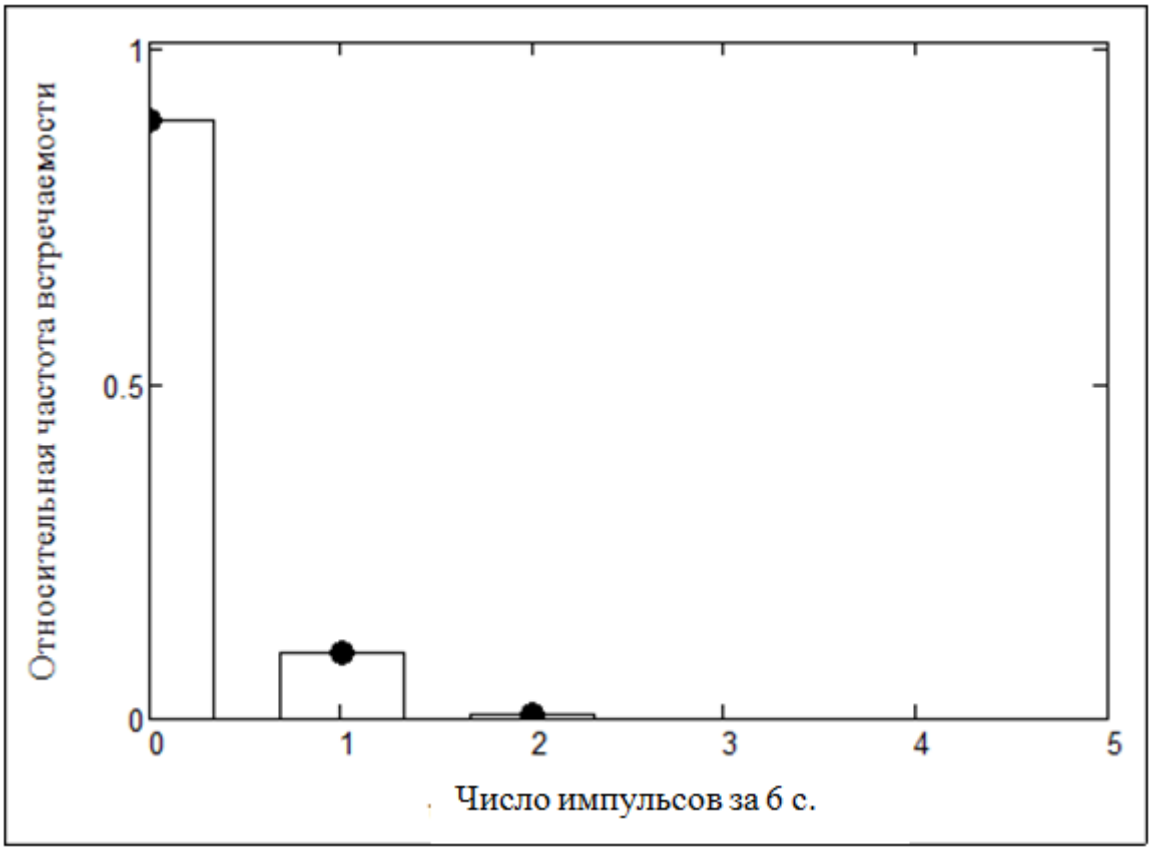
Относительная частота встречаемости
1
0.5
0
0
1
2
3
4
5
Число импульсов за 6 с.

Fig. 1.

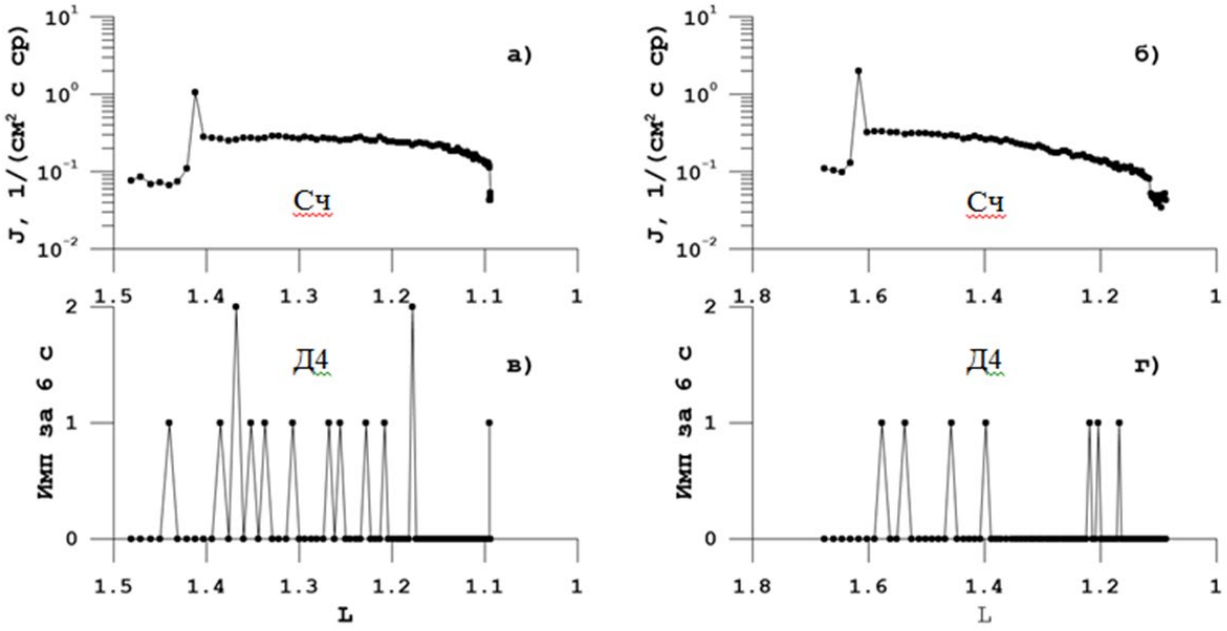

Fig. 2.

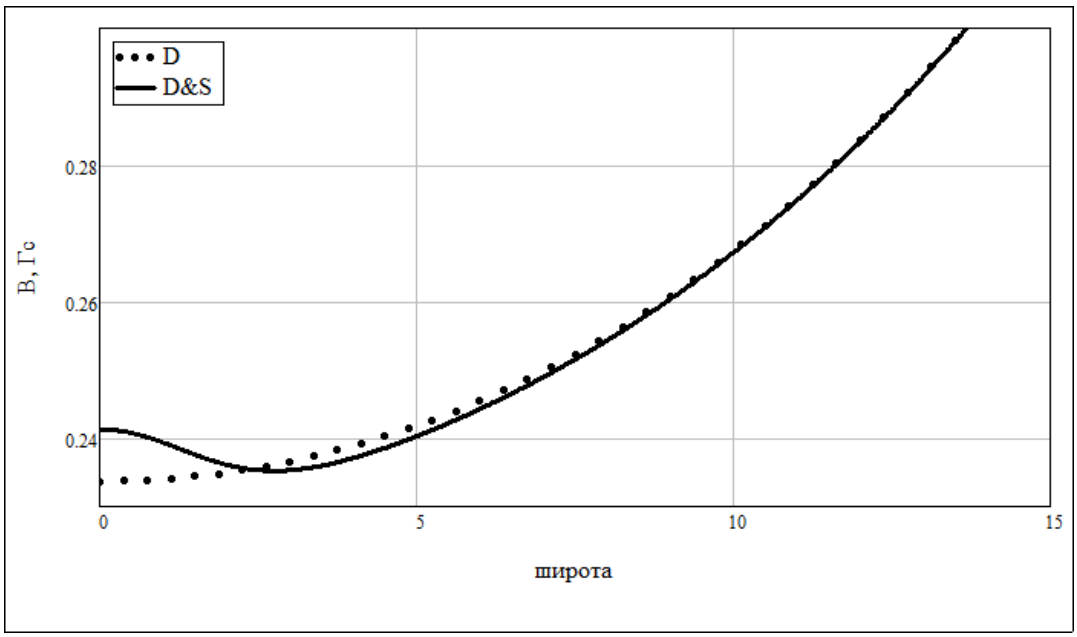

Fig. 3.

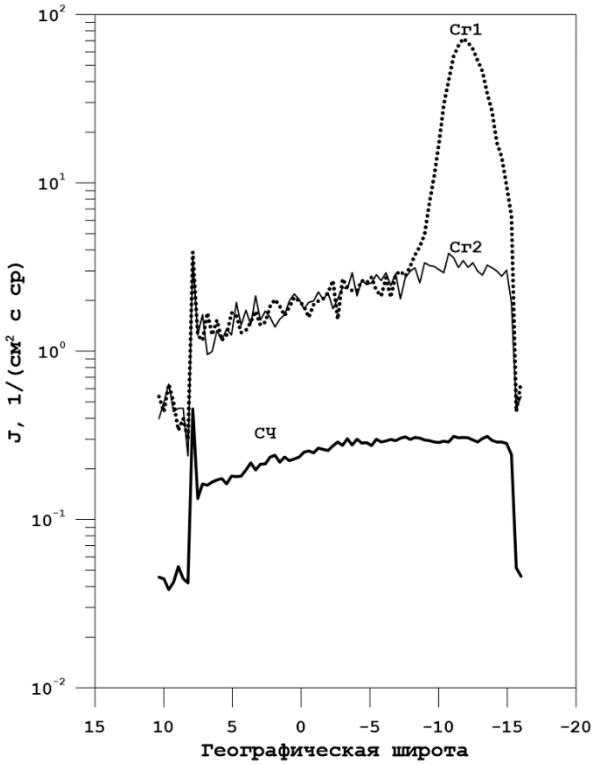

Fig. 4.